Supporting Information

Fénelon et al. 10.1073/pnas.1101219108

SI Text

Changes in the Excitatory Postsynaptic Potential Summation Are Not Due to Differences in Intrinsic Membrane Properties, Hyperpolarization-Activated Cyclic Nucleotide-Gated (HCN) Cation Channel Activation, or Firing Properties. Although decreased transmitter release may account for some of the difference in excitatory postsynaptic potential (EPSP) summation during a 50-Hz train, differences in intrinsic membrane properties could also contribute to this effect. Therefore, we determined whether the observed changes in synaptic plasticity could be a result of changes in some intrinsic neuronal properties. The resting membrane potentials of layer 5 (L5) pyramidal neurons were not different between genotypes (Table S2) (WT: $N = 13, n = 21$; *Dgcr8*$^{+/-}$: $N = 13; n = 27$; t tests; $P > 0.05$), nor were input resistances, capacitances, or rheobase (Table S2) (WT: $N = 13, n = 21$; *Dgcr8*$^{+/-}$: $N = 13; n = 27$; t tests; $P > 0.05$).

EPSP summation depends on EPSP decay time, which in turn depends, at least in part, on membrane time constant, τ (1). Thus, we determined whether *Dgcr8* deficiency affected this postsynaptic property by fitting a monoexponential to the initial part of the membrane potential trace hyperpolarized by a −30 pA current injection (Fig. S2*A*, *Inset*). We found no genotypic difference (Fig. S2*A*) (WT: $N = 13, n = 21$; *Dgcr8*$^{+/-}$: $N = 13; n = 27$; $P > 0.05$), consistent with the lack of effect on input resistance and capacitance.

Activation of hyperpolarization-activated cyclic nucleotide-gated (HCN) channels, located on pyramidal neuron dendrites in L5 of the medial prefrontal cortex (mPFC), has been shown to decrease synaptic summation in mice (2). To assess voltage-dependent HCN channel activation, we quantified the voltage sag ratio by dividing the steady-state hyperpolarization amplitude by the peak hyperpolarization in response to a 500-ms current injection of −150 pA (Fig. S2*B*). We found no difference between genotypes (WT: $N = 9, n = 13$; *Dgcr8*$^{+/-}$: $N = 8; n = 12$; t test; $P > 0.05$). The firing properties at increasing levels of current injection were also compared and were similar between genotypes (Fig. S2*C*) (WT: $N = 9, n = 13$; *Dgcr8*$^{+/-}$: $N = 8; n = 12$; t test; $P > 0.05$). Overall, the membrane properties of postsynaptic L5 pyramidal neurons tested here, such as the membrane time constant, the HCN channel activation, and cell excitability, do not seem to contribute to the genotypic difference in the amount of EPSP summation during synaptic depression.

SI Materials and Methods

Electrophysiological Recordings. During all recordings, the slices were continuously perfused with artificial cerebrospinal fluid (aCSF) (bubbled with 5% CO_2/95% O_2) that had the following composition (in mM): NaCl 124, KCl 2.5, NaH_2PO_4 1, $NaHCO_3$ 25, Glucose 10, $MgSO_4$ 1, $CaCl_2$ 2. The aCSF was maintained at 33 to 36 °C and fed by gravity at a rate of 2 to 3 mL per minute. Field EPSPs (fEPSPs) were recorded via a glass microelectrode (3–5 MΩ) filled with aCSF and placed in L5 of the mPFC (600–800 μm from midline). Whole-cell patch-clamp recordings of L5 pyramidal neurons in the mPFC were obtained using patch pipettes (3–5 MΩ) filled with (in mM): $KMeSO_4$ 125, KCl 10, Hepes 10, NaCl 4, EGTA 0.1, MgATP 4, Na_2GTP 0.3, Phosphocreatine 10, Biocytin 0.1% (pH = 7.2; osmolarity = 285–300 mosm). Cells having a voltage potential more negative than −65 mV, having overshooting action potentials, and showing spike-frequency adaptation only were used. The biocytin-filled recorded neurons had basal dendrites and a long apical dendrite extending to the superficial cortical layers where it branched extensively (3, 4).

Signals were acquired using the pClamp10 software, the Digidata 1440A (Molecular Devices) and an extracellular amplifier (Cygnus Technologies) (field recordings) or with a Multiclamp 700B amplifier (Molecular Devices) (patch-clamp experiments). Statistical analyses were done using the Sigmaplot and Statview softwares. A t test or a two-way repeated-measures ANOVA followed by post hoc testing was used to compare differences between genotypes. A confidence level of $P < 0.05$ was considered statistically significant. Data are presented as means ± SEM. N indicates number of animals, n indicates number of slices.

Immunohistochemistry, BrdU-Labeling, and Antibodies. Immunocytochemical analysis of laminar organization used brains from 6-wk-old males, perfused with PBS and 4% PFA, that were postfixed in PFA overnight. Vibratome sections (60-mm thickness) were washed three times in PBS and blocked in PBS with 0.4% Triton X-100 and goat serum at room temperature for 3 h. Primary antibodies were incubated overnight at 4 °C. After washing, samples were incubated with appropriate second antibodies for 3 h at room temperature. For BrdU-labeling, timed pregnant mice (E16.5) were injected intraperitoneally with BrdU (100 mg/kg body weight). Pups (P5) brains were collected at birth and fixed in 4% PFA overnight, and serial vibratome sections were collected. Sections were treated with 2 N HCl to expose the BrdU antigen. Quantification of first-generation BrdU-labeled cells and distribution within cortical layers were analyzed using established methods (5, 6). Primary antibodies used included the following: NeuN (mouse, 1:200, Affinity; BD Bioscience), Cux-1 antibody (rabbit, 1:50; Santa Cruz); BrdU (mouse, 1:200, BD Bioscience; rat, 1:300, AbD Serotec), CTIP2 (rat, 1:500; Abcam), TBR-1 (rabbit, 1:300; Abcam), TBR-2 (rabbit, 1:100; Abcam), PH3 (rat, 1:300; Abcam), All secondary antibodies (goat; Molecular Probes) were used at a concentration of 1:100.

Image Acquisition. ***Tissue sections.*** Confocal images of neurons were obtained blind to genotype with the LSM 510 using a Zeiss 20× objective with sequential acquisition setting at 2,048 × 2,048 pixel resolution. Each image was a z-series projection of approximately three to five images, and taken at 2.0-μm depth intervals using the same settings for pinhole size, brightness, and contrast. Data were analyzed by counting the number of puncta in a sampling of five consecutive optical sections in the stack. The region of interest in the frontal cortex was defined by a 71.4-μm × 64.2-μm box. The particle measurement feature was then used, with a same setting of minimal puncta size and threshold, to count the number of discrete puncta of the image. Puncta number and intensity were first averaged across optical sections and then compared statistically across regions of the frontal cortex, as well as genotype, using ANOVA. Images acquired for the NeuN and Cux-1 puncta analysis were taken with sequential acquisition setting at 2,048 × 2,048 pixel resolution as single image from the frontal cortex (dorsal, medial, and lateral regions of each coronal section) (Fig. S4). A total of 24 images from six male mice were analyzed for each genotype. The cortical layers were identified by CTIP2 (a L5 marker) and Cux1 (a L2/4 marker) immunostaining and the cortical thickness was divided into 10 bins (Bin 1: MZ and Layer 1; Bins 2 and 3: Layer 2–4; Bins 4 and 5: Layer 5; Bins 6–9: Layer 6; Bin 10: Subplate). Some bins in same layer were evenly divided. The region of interest was defined by a 300-μm line parallel to the cortical layer. The particle measurement feature was then used, with a same setting of

minimal puncta size and threshold, to count the number of discrete puncta in the image.

Analysis of Spine Morphology. *Dgcr8*$^{+/-}$ mice were crossed to the *Thy1-GFP/M* mouse line. Five *Dgcr8*$^{+/-}$*;Thy1-GFP/M*$^{+/-}$ and five WT *Thy1-GFP/M*$^{+/-}$ littermates, 8-wk-old, were perfused with 4% paraformaldehyde, their brains were dissected and 100-μm sections were generated using a vibratome (Leica). Prefrontal cortex neuron images were acquired on a Zeiss LSM 510 laser-scanning confocal microscope. For each experiment, images across all genotypes were acquired with similar optimal settings for laser power, detector gain, and amplifier offset with a pinhole diameter equivalent to one Airy unit for the 488-nm laser. Twelve-bit images were obtained using a 63× objective at a resolution of 2,048 × 2,048 pixels. Images were acquired as a *z*-stack, and a maximum intensity projection of each neuron was created from the *z*-stack using 60 to 80 sections (0.14 μm per section). Quantification of spine density, length, and width was performed first with auto tracing and followed by manual correction using Neuron Studio Software (7). One basal dendrite, at least 75 μm in length, was analyzed from each prefrontal cortex neuron, as described previously (6). We analyzed four or five neurons for each animal. In total, we quantified 49 neurons (24 from *Dgcr8*$^{+/-}$ and 25 from WT mice) and 1,858 spines (877 from *Dgcr8*$^{+/-}$ and 981 from WT mice). The length of the entire spine (including head and neck) was measured as the distance of a straight line with the shortest distance from the furthest tip of the spine head to the dendritic shaft. Spine width was measured as the distance of a straight line drawn across the widest part of the spine head. Total spine density was assessed by student's *t* test. Distributions of the length and width of mushroom spines were compared using the Kolmogorov-Smirnov test.

Analysis of Dendritic Complexity. We acquired prefrontal cortex neuron images as described in the previous section, using a 40× objective at a resolution of 1,024 × 1,024 pixels. Images were acquired as a *z*-stack and a maximum intensity projection of each neuron was created from the *z*-stack using 120 to 160 sections (0.45 μm per section). The raw projected 2D images were imported into Neuron Studio software. All basal dendrite branches from the soma were traced with auto tracing function and followed by manual correction in Neuron Studio (8). The tracing images were then imported into ImageJ (http://rsb.info.nih.gov/ij/) and analyzed using Sholl Analysis Plugin (http://biology.ucsd.edu/labs/ghosh/software/) with a "radius step size" of 5 μm. The points where the dendrites crossed the lines of concentric rings were taken as intersecting points. We counted the number of dendritic branching points and intersections in successive radial segments of 5 μm by considering the center of the soma as a reference point. The .SWC tracing files generated by Neuron Studio, which carry all dendritic structure information, were imported into L-measure software to measure different dendritic features such as the number of primary dendrites, number of branches, and total length (9).

1. Wessel R, Kristan WB, Jr., Kleinfeld D (1999) Supralinear summation of synaptic inputs by an invertebrate neuron: dendritic gain is mediated by an "inward rectifier" K+ current. *J Neurosci* 19:5875–5888.
2. Day M, Carr DB, Ulrich S, Ilijic E, Tkatch T, et al. (2005) Dendritic excitability of mouse frontal cortex pyramidal neurons is shaped by the interaction among HCN, Kir2, and Kleak channels. *J Neurosci* 25:8776–8787.
3. Kawaguchi Y (1993) Groupings of nonpyramidal and pyramidal cells with specific physiological and morphological characteristics in rat frontal cortex. *J Neurophysiol* 69:416–431.
4. Yang CR, Seamans JK, Gorelova N (1996) Electrophysiological and morphological properties of layers V-VI principal pyramidal cells in rat prefrontal cortex in vitro. *J Neurosci* 16:1904–1921.
5. Molyneaux BJ, Arlotta P, Hirata T, Hibi M, Macklis JD (2005) Fezl is required for the birth and specification of corticospinal motor neurons. *Neuron* 47:817–831.
6. Lai T, et al. (2008) SOX5 controls the sequential generation of distinct corticofugal neuron subtypes. *Neuron* 57:232–247.
7. Rodriguez A, Ehlenberger DB, Dickstein DL, Hof PR, Wearne SL (2008) Automated three-dimensional detection and shape classification of dendritic spines from fluorescence microscopy images. *PLoS ONE* 3:e1997.
8. Wearne SL, et al. (2005) New techniques for imaging, digitization and analysis of three-dimensional neural morphology on multiple scales. *Neuroscience* 136:661–680.
9. Scorcioni R, Polavaram S, Ascoli G (2008) L-Measure: A web-accessible tool for the analysis, comparison and search of digital reconstructions of neuronal morphologies. *Nat Protoc* 3:866–876.

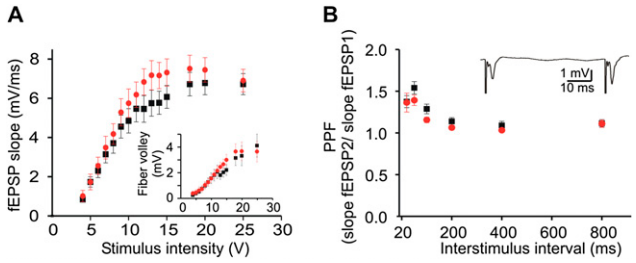

Fig. S1. The effect of the *Dgcr8* deficiency on basic synaptic transmission and short-term synaptic facilitation in L5 of the mPFC. (*A*) The input-output relation across experiments as well as the afferent volley amplitude (*Inset*) are normal in *Dgcr8*$^{+/-}$ mice (two-way repeated-measures ANOVA; $P > 0.05$). WT mice ($N = 7$; $n = 17$). *Dgcr8*$^{+/-}$ mice ($N = 7$; $n = 17$). (*B*) Paired-pulse facilitation (PPF) is normal in *Dgcr8*$^{+/-}$ mice at various interstimulus intervals (two-way repeated-measures ANOVA; $P > 0.05$). WT mice ($N = 7$; $n = 17$); *Dgcr8*$^{+/-}$ mice ($N = 7$; $n = 17$). A paired-pulse sample trace is shown at the top of the panel.

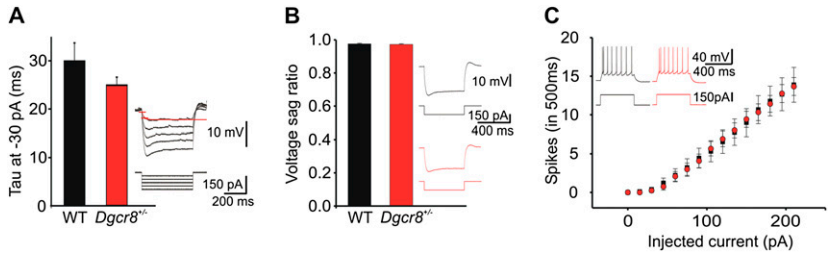

Fig. S2. Measures of basic intrinsic properties of L5 pyramidal neurons of the mPFC of *Dgcr8*$^{+/-}$ mice. (*A*) The membrane time constant, τ (ms) was measured by fitting a monoexponential (*Inset*, red trace) on the initial hyperpolarizing phase of the membrane potential induced by a −30 pA current injection. The *Dgcr8* deficiency does not affect the membrane time constant (WT: $N = 13$, $n = 21$; *Dgcr8*$^{+/-}$: $N = 13$, $n = 27$; *t* test, $P > 0.05$). (*B*) As illustrated by the sample traces on the right, the voltage sag ratio measured by a 500-ms current injection of −150 pA is unchanged by the mutation (WT: $N = 9$, $n = 13$; *Dgcr8*$^{+/-}$: $N = 8$, $n = 12$; *t* test, $P > 0.05$). (*C*) The intrinsic excitability is normal in *Dgcr8* heterozygous mutant mice (WT: $N = 9$, $n = 13$; *Dgcr8*$^{+/-}$: $N = 8$, $n = 12$; *t* test, $P > 0.05$) as shown by the sample traces obtained by a 500-ms depolarizing current injection of +150 pA. Data presented as means ± SEM.

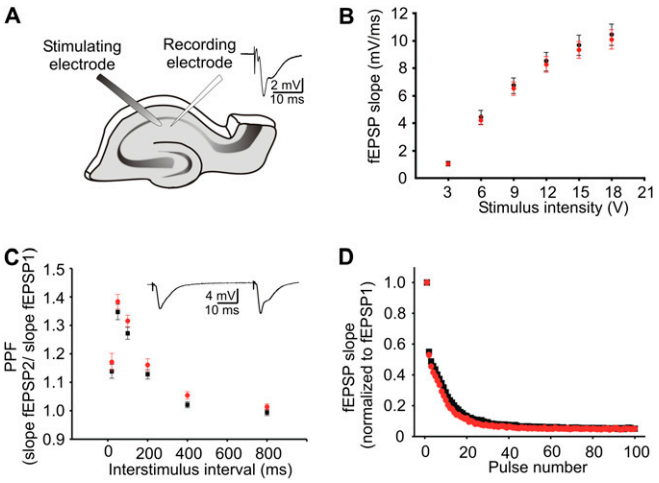

Fig. S3. The effect of the *Dgcr8* mutation on synaptic transmission and plasticity in CA1. (*A*) Schematic illustration of the transverse hippocampal slice. Extracellular field recordings were made by stimulating the Schaffer collateral fibers and recording from stratum radiatum in CA1. A sample fEPSP trace is illustrated on the right. (*B*) The mean fEPSP initial slopes show that the stimulus-response relation is not affected by the mutation. WT mice ($N = 5$; $n = 40$); *Dgcr8*$^{+/-}$ mice ($N = 5$; $n = 38$). (*C*) There is no significant difference in release probability as assessed by the PPF between WT ($N = 5$, $n = 37$) and *Dgcr8*$^{+/-}$ mice ($N = 5$, $n = 36$). (*D*) Depression of the fEPSP slopes recorded during two 100-Hz trains (100 pulses, 1 s) is similar between genotypes. WT mice ($N = 5$; $n = 24$); *Dgcr8*$^{+/-}$ mice ($N = 5$; $n = 20$). Data presented as means ± SEM.

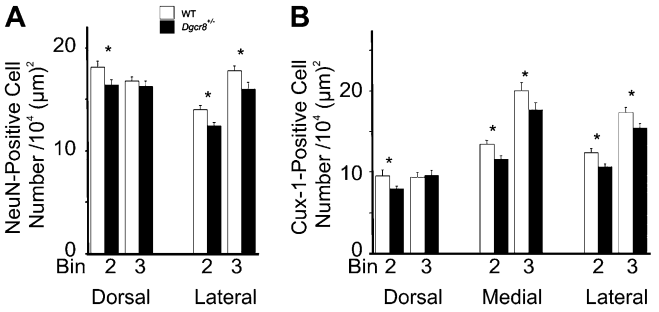

Fig. S4. Modest decrease in L2/4 cell frequency in the cortex of *Dgcr8*$^{+/-}$ mice. (*A*) NeuN L2/4-labeled neurons in dorsal and lateral frontal cortex in 6-wk-old WT and *Dgcr8*$^{+/-}$ mice. ($n = 18$ per genotype). (*B*) Cux1 L2/4-labeled neurons in dorsal, medial, and lateral frontal cortex in 6-wk-old WT and *Dgcr8*$^{+/-}$ mice ($n = 18$ per genotype). Frequency of NeuN- and Cux1-labeled cells is represented as number of cells per 10^4 mm^2. Data presented as means ± SEM. *$P < 0.05$.

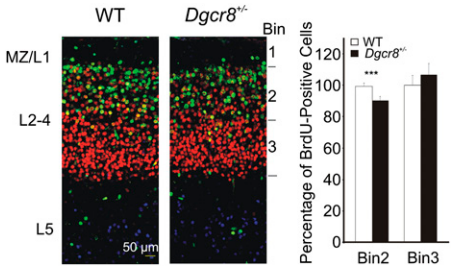

Fig. S5. Late corticogenesis is impaired in the cortex of *Dgcr8*$^{+/-}$ mice. Reduction of BrdU-labeled cells in the P5 cortex after a single pulse of BrdU at E16.5 in WT and *Dgcr8*$^{+/-}$ mice. (n = 18 per genotype). The cortical thickness was divided into 10 equal bins from pia to white matter, and the distribution of BrdU-labeled cells across the bins 2 and 3 was determined. Quantification of BrdU^{+} cells born at E16.5 showed a significant decrease in superficial L2/4 between WT and *Dgcr8*$^{+/-}$ mice. Cells scored as BrdU^{+} (green) in matched 300-μm wide sections of the P5 cortex (BrdU labeled at E16.5). Cortical layers were identified by Cux1 (red: L2-3 marker) and CTIP2 (blue: L5 marker). Bin 2 and Bin 3 were equally divided. Data presented as means ± SEM. ***$P < 0.0001$.

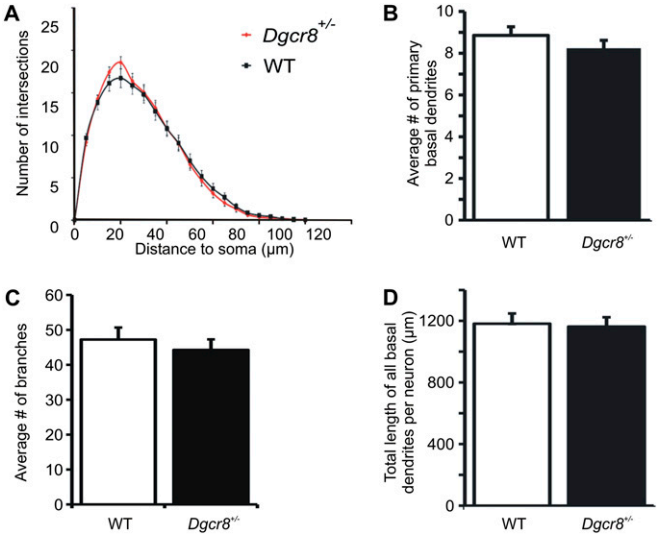

Fig. S6. *Dgcr8* deficiency does not affect dendritic morphology, complexity or dendritic spine length in L5 pyramidal neurons of the mPFC. (*A*) Sholl analysis using 5-μm concentric circles around the soma showing normal dendritic complexity of basal dendrites of L5 pyramidal neurons of *Dgcr8*$^{+/-}$*Thy1-GFP/M*$^{+/-}$ (N = 5, n = 24) relative to WT *Thy1-GFP/M*$^{+/-}$ (N = 5, n = 25). Branching appears normal toward the soma and at distances up to 100 μm from the soma. Data are shown as means ± SEM. (*B*) The number of primary dendrites and (*C*) the number of branches were normal in *Dgcr8*$^{+/-}$*Thy1-GFP/M*$^{+/-}$. (*D*) The length of basal dendrites was unaffected by the mutation. WT *Thy1-GFP/M*$^{+/-}$ (N = 5, n = 981). *Dgcr8*$^{+/-}$*Thy1-GFP/M*$^{+/-}$ (N = 5, n = 877).

Table S1. Properties of sEPSC recorded in L5 pyramidal neurons of WT and *Dgcr8*$^{+/-}$ mice

	Wild type	*Dgcr8*$^{+/-}$
Amplitude (pA)	22.1 ± 1.3	21.5 ± 0.8
Decay time (ms)	4.4 ± 0.4	4.6 ± 0.3
Area (pA*ms)	90.0 ± 6.6	92.0 ± 5.2
Rise time (ms)	1.4 ± 0.1	1.5 ± 0.1
No. of events/5 min	344 ± 85	277 ± 46

Table S2. Intrinsic properties of L5 pyramidal neurons of WT and *Dgcr8*$^{+/-}$ mice

	Wild type	*Dgcr8*$^{+/-}$
Resting voltage potential (mV)	−71.2 ± 1.3	−71.2 ± 1.1
Input resistance (Mohms)	212.6 ± 24.8	213.6 ± 20.9
Capacitance (pF)	75.8 ± 5.7	76.8 ± 4.9
Rheobase (pA)	83 ± 11	69 ± 7